HEFAT2011
8th International Conference on Heat Transfer, Fluid Mechanics and Thermodynamics
26 June – 1 July 2011
Pointe Aux Piments, Mauritius

OPTIMUM OPERATING CONDITIONS OF THE SMALL-SCALE OPEN AND DIRECT SOLAR THERMAL BRAYTON CYCLE AT VARIOUS STEADY-STATE CONDITIONS

Le Roux, W.G., Bello-Ochende*, T. and Meyer J.P.
*Author for correspondence
Department of Mechanical and Aeronautical Engineering,
University of Pretoria,
Pretoria, 0002,
South Africa,
E-mail: tunde.bello-ochende@up.ac.za

ABSTRACT

A heat source can be considered as the Brayton cycle's life support. This heat source can be extracted from solar energy. The small-scale open and direct solar thermal Brayton cycle with recuperator has several advantages, including lower cost, low operation and maintenance costs and it is highly recommended. The main disadvantages of this cycle are the pressure losses in the recuperator and receiver, turbo-machine efficiencies and recuperator effectiveness, which limit the net power output of such a system. The irreversibilities of the solar thermal Brayton cycle are mainly due to heat transfer across a finite temperature difference and fluid friction. Thermodynamic optimization can be applied to address these disadvantages to optimize the receiver and recuperator and to maximize the net power output of the system at any steady-state condition. The dynamic trajectory optimization method is applied to maximize the net power output of the system by optimizing the geometries of the receiver and recuperator limited to various constraints. Standard micro-turbines and parabolic dish concentrator diameters of 6 to 18 meters are considered. An optimum system geometry and maximum net power output is generated for each operating condition of each micro-turbine and concentrator combination. Results show the optimum operating conditions as a function of system mass flow rate. The optimum operating point of a specific micro-turbine is at a point where the internal irreversibilities are approximately three times the external irreversibilities. For a specific environment and parameters there exists an optimum receiver and recuperator geometry so that the system produces maximum net power output.

NOMENCLATURE

a	[m]	Longer side of rectangular recuperator channel
A	[m^2]	Area
b	[m]	Shorter side of rectangular recuperator channel
c_{p0}	[J/kgK]	Zero pressure constant pressure specific heat
CR	[-]	Concentration ratio (D_{conc}/d)
C_W	[-]	Optimum ratio of minimum irreversibility rate
d	[m]	Receiver aperture diameter
D	[m]	Receiver diameter
D_{conc}	[m]	Parabolic dish concentrator diameter
D_{rec}	[m]	Receiver tube diameter
$D_{h,reg}$	[m]	Hydraulic diameter of recuperator channel
e_p	[rad]	Parabolic concentrator error
f	[-]	Friction factor
Gr	[-]	Grashof number
h	[W/m^{2}K]	Heat transfer coefficient
h	[-]	Increment of variable value
H	[m]	Recuperator height
I	[W/m^2]	Solar Irradiance
$\dot{I}$	[W]	Rate of Irreversibility
k	[W/mK]	Thermal conductivity of a fluid
k	[-]	Gas constant (c_p / c_v)
L	[m]	Length
$\dot{m}$	[kg/s]	System mass flow rate
$\dot{m}_c$	[kg/s]	Recuperator channel mass flow rate
MT	[-]	Micro-turbine model number (1 – 45)
n	[-]	Number of flow channels
NTU	[-]	Number of transfer units
Nu	[-]	Nusselt number
P	[Pa]	Pressure
Pr	[-]	Prandtl number
$\dot{Q}*$	[W]	Rate of intercepted heat at receiver cavity
$\dot{Q}_{loss}$	[W]	Rate of heat loss from the cavity receiver
$\dot{Q}_{net}$	[W}	Net rate of absorbed heat
r	[-]	Compressor pressure ratio
$refl$	[-]	Specular reflectivity
R	[J/kgK]	Gas constant
Re	[-]	Reynolds number
R_f	[-]	Fouling factor
$\dot{S}_{gen}$	[W/K]	Entropy generation rate
t	[m]	Plate thickness between recuperator flow channels
T	[K]	Temperature
$T*$	[K]	Apparent sun temperature as an exergy source
T_0	[K]	Environment temperature
V	[m/s]	Velocity
w	[-]	Wind factor

$\dot{W}$	[W]	Power
$\dot{W}_{net}$	[W]	Net power output of system
X	[-]	Optimisation vector with five geometry variables
y	[-]	Numerical approximation constant
Z	[m]	Height
β	[-]	Inclination of receiver
ε	[-]	Effectiveness (in the *ε-NTU* method)
ρ	[kg/m^3]	Density
φ_{rim}	[-]	Concentrator rim angle
μ	[kg/ms]	Dynamic viscosity

Subscripts

0	Environment/Loss
1,2,3..	Refer to Figure 1
c	Compressor
a	Receiver aperture
conc	Concentrator
conv	Due to convection
D	Based on internal diameter of channel
ext	External
h	Hydraulic
high	Highest on island of maximum compressor efficiency
int	Internal
low	Lowest on island of maximum compressor efficiency
max	Maximum
min	Minimum
opt	Optimum
rad	Due to radiation
rec	Receiver
reg	Recuperator
s	Surface
t	Turbine
w	Receiver inner wall

1. INTRODUCTION

Concentrated solar power systems use the concentrated power of the sun as a heat source to generate mechanical power. Air can be used as the working fluid in the Brayton cycle. The Brayton cycle is definitely worth studying when comparing its efficiency with those of other power cycles [1]. Emphasis may shortly shift to solarised Brayton micro-turbines from Dish-Stirling technology due to high Stirling engine costs [2]. When a recuperator is used the Brayton cycle has very high efficiency at low pressure ratios. The main disadvantages of a solar thermal Brayton cycle are the pressure losses in the recuperator and receiver, turbomachine efficiencies and recuperator effectiveness [3], which limit the net power output of such a system. Maximum net power output is required for a small-scale solar thermal Brayton cycle with recuperator. The net power output can for example be used to drive an electrical generator and the higher the net power output the more electricity can be produced. To obtain this maximum net power output, a combined effort of heat transfer, fluid mechanics and thermodynamic thought is required. The method of entropy generation minimisation combines these thoughts [4].

The irreversibilities of the recuperative solar thermal Brayton cycle are mainly due to heat transfer across a finite temperature difference and fluid friction. Various authors have emphasised the importance of the optimisation of the global performance of a system, by minimising the total irreversibility rate from all the different components or processes of the system by sizing the components accordingly [5-11]. For the open and direct solar thermal Brayton cycle, an optimisation of this kind is not available from the literature. The geometries of the receiver and recuperator can be optimised in such a way that the total entropy generation rate is minimised to allow maximum net power output at any steady-state condition.

The exact exergy of solar radiation depends on direct and diluted radiation components, the time of day, season of the year, geographic location, local weather and landscape and could be determined with spectral measurement and calculation [12] or solar exergy maps [13].

Entropy generation minimisation (EGM) has been used in various internal flow optimisation studies such as: The optimum tube diameter or Reynolds number for a tube [5,7]; the optimal Reynolds number for single-phase, fully developed, laminar and turbulent flow with constant heat flux [14]; and the optimum channel geometries with constant wall temperature or constant heat flux [10-11]. Entropy generation and its minimisation has also been expressed for numerous heat exchangers and heat transfer surfaces: counterflow and nearly-ideal heat exchanger neglecting fluid friction [15], tubular heat exchangers [16,17], heat exchangers restricted to perfect gas flows [18], balanced cross-flow recuperative plate type heat exchangers with unmixed fluids [19]; and a parallel-plates ideal gas counterflow heat exchanger [8]. The *ε-NTU* method, based on the second law of thermodynamics, can be used to get the outlet temperatures and the total heat transfer from the hot fluid to the cold fluid in a heat exchanger [8,18,19].

When mounting a black solar receiver at the focus of a parabolic dish concentrator it can be sized such that it absorbs the maximum amount of heat [3]. Convection losses can be drastically reduced with the use of a cavity receiver. Different types of cavity receivers have been compared [20-22]. The modified cavity receiver is suggested by Sendhil Kumar and Reddy [22] since it experiences lower convection heat losses. For the modified cavity receiver, a numerical investigation of natural convection heat loss is available [23], the contribution of radiation losses is considered [24] and an improved model for natural convection heat loss is available [25].

Exergetic analysis for a regenerative Brayton cycle with isothermal heat addition and isentropic compressor and turbine [26] is available.

In this paper the geometries of a modified cavity receiver [22-25] and counterflow plate-type recuperator [27] are optimised so that the system produces maximum net power output at any steady-state environment.

The total entropy generation rate in the system is minimised, instead of optimising components individually. The dynamic trajectory optimisation method for constrained optimisation [28] is used. Off-the-shelf micro-turbines [29] chosen for low cost, high availability and reliability and a range of parabolic dish concentrator diameters are considered. The effect of various environmental conditions and constraints on the optimum geometries is investigated.

The net power output of the system is maximised, the total entropy generation rate is minimised and the geometries of the receiver and recuperator are optimised.

2. MODEL

The open and direct solar thermal Brayton cycle with recuperator is shown in Figure 1. A parabolic concentrator concentrates the solar heat for the cavity receiver.

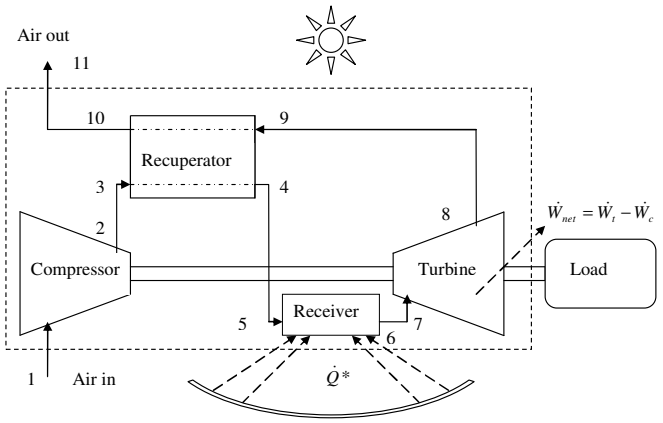

Figure 1 The open and direct solar thermal Brayton cycle with recuperator.

2.1. The control volume

The rate of intercepted heat by the cavity receiver, $\dot{Q}^*$, depends on the cavity receiver aperture (which depends on the geometries of the cavity receiver). For the analysis in this work, T^* will be assumed to be 2 470 K [4] and at a point between the concentrator and receiver. $\dot{Q}^*$ can be regarded as the intercepted power at the receiver, after the irreversibility rates due to scattering and the transformation of monochromatic radiation have been deducted. $\dot{W}_{net}$ is the net power output of the system.

2.2. Solar receiver model

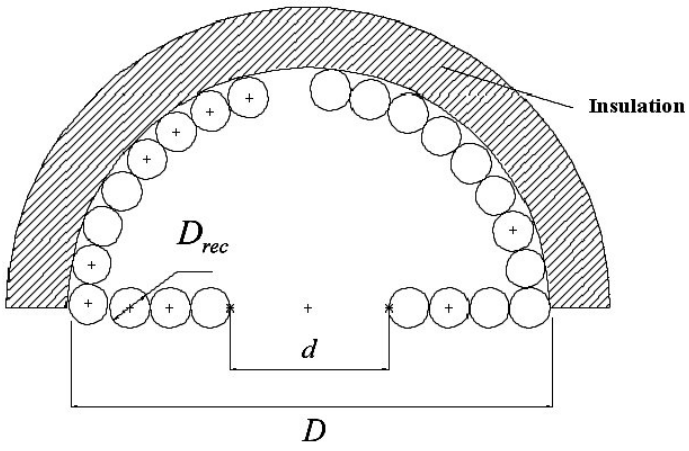

Figure 2 Modified cavity receiver.

The modified cavity receiver suggested by Reddy and Sendhil Kumar [25] is considered in the analysis and is shown in Figure 2. The receiver inner surface is made up of closely wound copper tubing with diameter, D_{rec} through which the working fluid travels. The receiver tube with length, L_{rec}, constructs the cavity receiver and its aperture. An area ratio of $A_w / A_a = 8$ is recommended [25] as it was found to be the ratio that gives the minimum heat loss from the cavity receiver. The convection heat loss takes place through the receiver aperture. Since the surface area of a sphere is πD^2, the diameter of the spherical receiver can be calculated as

$$D = 2\sqrt{(A_w + A_a)/3\pi} \tag{1}$$

Due to the area ratio constraint, the receiver diameter is a function of the receiver aperture diameter,

$$D = \sqrt{3}d \tag{2}$$

The receiver aperture diameter can be calculated using equation (3) since $A_w = D_{rec}L_{rec}$.

$$d = \sqrt{D_{rec}L_{rec}/2\pi} \tag{3}$$

According to Reddy and Sendhil Kumar [25], for $A_w / A_a = 8$, the Nusselt number for natural convection heat loss based on receiver diameter for a 3-D receiver model can be calculated as a function of the inclination angle of the receiver,

$$Nu_D = h_{conv}D/k = 0.698Gr_D^{0.209}(1+\cos\beta)^{0.968}(T_w/T_0)^{-0.317}(d/D)^{0.425} \tag{4}$$

For $A_w / A_a = 8$ and a 0° tilt angle (vertical aperture plane), the ratio of radiation heat loss to convection heat loss is a function of receiver inclination and varies between approximately 0.9 and 1.33. [25]. It is therefore assumed that $\dot{Q}_{loss,rad} \approx \dot{Q}_{loss,conv}$ or $\dot{Q}_{loss} \approx 2\dot{Q}_{loss,conv}$ for the modified cavity receiver. The total rate of heat loss due to convection and radiation, can therefore be approximated as

$$\dot{Q}_{loss} \approx 1.396Gr_D^{0.209}(1+\cos\beta)^{0.968}(T_w/T_0)^{-0.317}(d/D)^{0.425}(kA_a/D)(T_w - T_0) \tag{5}$$

The rate of conduction heat loss is assumed 10% of the sum of the radiation and convection heat loss rates.

2.3. Determination of net absorbed power

In practise, reflected rays from a solar concentrator form an image of finite size centred about its focal point. This is due to the sun's rays not being truly parallel and due to concentrator errors. Different concentrator sizes (6 – 18 m diameter) are used in the analysis. For a specific concentrator with constant diameter, focal length and rim angle, the net rate of heat absorbed by the working fluid in the receiver depends on the receiver aperture diameter. The larger the receiver aperture diameter, the larger the rate of heat intercepted by the receiver, $\dot{Q}^*$. Also, the larger the aperture diameter, the larger the heat loss rate, $\dot{Q}_{loss}$, due to convection and radiation in equation (5).

The net rate of absorbed heat, $\dot{Q}_{net}$, is the intercepted heat rate minus the total heat loss rate.

The sizing algorithm of Stine and Harrigan [3] is applied to determine $\dot{Q}*$ for a specific aperture diameter. Starting at a rim angle of 0° through to an angle of φ_{rim}, in increments of 1°, the amount of intercepted solar energy per segment of concentrator area is computed. The sizing algorithm uses the concentrator area, rim angle (φ_{rim}), specular reflectance, inclination, irradiance, parabolic concentrator error and heat loss to determine the net absorbed heat rate as a function of the receiver aperture diameter.

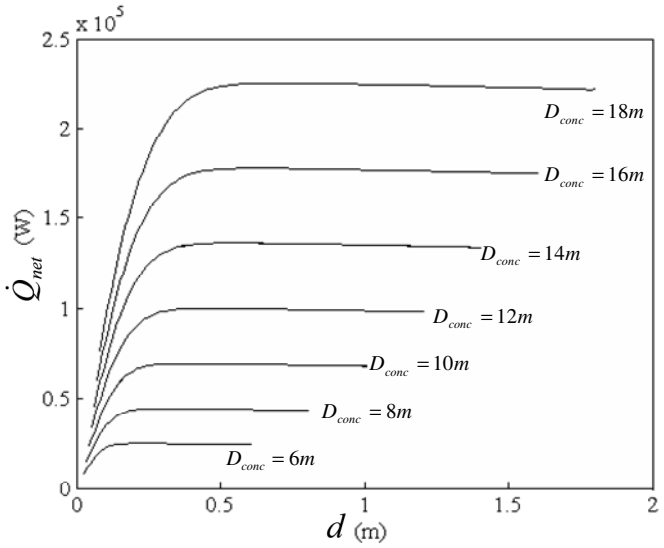

Figure 3 Net absorbed heat rate at cavity receiver depending on cavity receiver aperture diameter.

Figure 3 shows this relation between $\dot{Q}_{net}$ and the receiver aperture diameter for a number of different concentrator diameters. Note that Figure 3 was generated by using the default values (shown in Table 1), for the parabolic concentrator error [3], rim angle, receiver inclination, etc. The shadow of the receiver and its insulation is also accounted for when calculating the intercepted power. Each curve in Figure 3 can be numerically approximated with equation (6) using the discrete least squares approximation method [30], where y_i is a set of constants used to describe the function.

$$\dot{Q}_{net} = \sum_{i=0}^{10} y_i d^i \tag{6}$$

2.4. Recuperator model

A counterflow plate-type recuperator is used as shown in Figure 4. The channels with hydraulic diameter, $D_{h,reg}$, length, L_{reg}, and aspect ratio, a/b_{reg} are shown. The number of flow channels in the recuperator, n, depends on the recuperator height, H, channel height, b, and thickness of the channel separating surface, t, and can be written as a function of the channel aspect ratio,

$$n = H/(t+b) = \frac{H}{t + D_{h,reg}\left((a/b)_{reg}+1\right)/\left(2(a/b)_{reg}\right)} \tag{7}$$

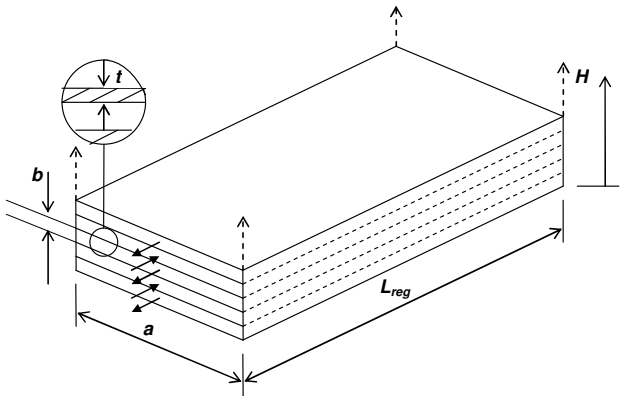

Figure 4 Counterflow plate-type recuperator.

Equation (8) gives the mass flow rate per channel.

$$\dot{m}_c = 2\dot{m}/n \tag{8}$$

The surface area, A_s, for a channel as a function of the channel aspect ratio is

$$A_s = 2(a+b)L_{reg} = D_{h,reg}L_{reg}\left((a/b)_{reg}+1\right)\left(1+(a/b)_{reg}^{-1}\right) \tag{9}$$

The thickness of the material between the hot and cold stream, t, is 1 mm. The Reynolds number for a flow channel is

$$\mathrm{Re} = \dot{m}_c D_{h,reg}(a/b)_{reg}/\mu a^2 \tag{10}$$

Using the definition of the hydraulic diameter and equation (10), the Reynolds number can be calculated with

$$\mathrm{Re} = \frac{4(a/b)_{reg}\dot{m}_c}{\mu D_{h,reg}\left((a/b)_{reg}+1\right)^2} \tag{11}$$

Heat exchanger irreversibilities can be reduced by slowing down the movement of fluid through a heat exchanger [4]. Small Reynolds numbers can thus be expected for the optimised recuperator channels and the Gnielinski equation [31] can be used to determine the Nusselt number,

$$Nu_D = \left(\mathrm{Pr}(\mathrm{Re}-1000)(f/8)\right)/\left(1+12.7(f/8)^{0.5}\left(\mathrm{Pr}^{2/3}-1\right)\right) \tag{12}$$

The Petukhov equation [32] is used to calculate the friction factor,

$$f = (0.79\ln\mathrm{Re}-1.64)^{-2} \tag{13}$$

With the use of the friction factor, Reynolds number and the definition of the pressure drop [33], the pressure drop through

the recuperator can be written in terms of the geometric variables as

$$\Delta P = \left(0.79 \ln \frac{4\dot{m}_c (a/b)_{reg}}{\mu D_{h,reg} (a/b_{reg} + 1)^2} - 1.64 \right)^{-2} \left(\frac{8\dot{m}_c{}^2 (a/b)_{reg}{}^2}{\rho (a/b_{reg} + 1)^4} \right) \left(L_{reg} / D_{h,reg}{}^5 \right) \tag{14}$$

The recuperator efficiency is calculated using the ε-*NTU* method with the fouling factor for air given as $R_f = 0.004$ [33].

2.5. Compressor and turbine properties

Forty-five standard micro-turbines are used in the analysis. The compressor pressure ratio ($r = P_2 / P_1$) can be chosen to be a parameter when considering geometric optimisation [34]. The mass flow rate through the system depends on the compressor, which in turn depends on the turbine of the micro-turbine. The compressor efficiency, mass flow rate and compressor pressure ratio, are intrinsically coupled to each other, when considering standard micro-turbines from Honeywell [29]. The compressor pressure ratio as a parameter, fixes the mass flow rate and compressor efficiency as parameters. The highest compressor efficiency is on the island in the middle of a compressor map (between two mass flow rate values: $\dot{m}_{low}$ and $\dot{m}_{high}$, and between two pressure ratio values: r_{low} and r_{high}). Different operating points on the island of maximum compressor efficiency of a micro-turbine can be considered with the straight line approximation of

$$\dot{m} = \frac{(\dot{m}_{high} - \dot{m}_{low})}{(r_{high} - r_{low})} (r - r_{low}) + \dot{m}_{low} \tag{15}$$

An optimum operating condition, for a specific micro-turbine, exists which would (with its optimised geometry) give the highest maximum net power output for the system. The operating conditions are used as parameters in the objective function. The maximum of the objective function can be found at different parameter values.

2.6. The objective function

The objective function is the function which is maximised by the optimisation of variables. The net power output of the system should be written in terms of the total entropy generation rate in the system. The entropy generation mechanisms are identified and the objective function is constructed.

2.6.1. Temperatures and pressures in terms of geometry variables

The objective function requires the values of the temperatures and pressures at each point in Figure 1. An iteration is required. Firstly, T_1 = 300 K and $P_1 = P_{10} = P_{11}$ = 80 kPa (see Figure 1). The temperatures and pressures in all the ducts are calculated with an assumed temperature loss or pressure drop which is small. The iteration starts off with T_5 = 800 K. Equations (16) - (19) and the recuperator efficiency are employed to calculate the remaining unknowns to produce a new approximation for T_5. The iteration continues until the error is smaller than 1×10^{-3}.

$$T_6 = \left(\sum_{i=0}^{10} a_i \sqrt{D_{h,rec} L_{rec} / 2\pi}^{\,i} \right) / \dot{m} c_{p0} + T_5 \tag{16}$$

$$P_4 = P_3 - \left(0.79 \ln \frac{4\dot{m}_c (a/b_{reg})}{\mu D_{h,reg} (a/b_{reg} + 1)^2} - 1.64 \right)^{-2} \left(\frac{8\dot{m}_c{}^2 (a/b_{reg})^2}{\rho (a/b_{reg} + 1)^4} \right) \left(\frac{L_{reg}}{D_{h,reg}{}^5} \right) \tag{17}$$

$$P_6 = P_5 - \left(0.79 \ln \frac{4\dot{m}}{\mu \pi D_{h,rec}} - 1.64 \right)^{-2} \left(\frac{8\dot{m}^2}{\rho \pi^2} \right) \left(\frac{L_{rec}}{D_{h,rec}{}^5} \right) \tag{18}$$

$$P_9 = P_{10} + \left(0.79 \ln \frac{4\dot{m}_c (a/b_{reg})}{\mu D_{h,reg} (a/b_{reg} + 1)^2} - 1.64 \right)^{-2} \left(\frac{8\dot{m}_c{}^2 (a/b_{reg})^2}{\rho (a/b_{reg} + 1)^4} \right) \left(\frac{L_{reg}}{D_{h,reg}{}^5} \right) \tag{19}$$

2.6.2. Construction of the objective function

When the maximum net power output that can be delivered by the system is required, the total entropy generation rate in the system should be considered. The finite heat transfers and pressure drops in the compressor, turbine, recuperator, receiver and ducts are identified as entropy generation mechanisms. When doing an exergy analysis for the system and assuming $V_1 = V_{11}$ and $Z_1 = Z_{11}$, the objective function can be assembled as given in equation (20). The function to be maximised (the objective function), is $\dot{W}_{net}$ (the net power output). Equation (21) shows the total entropy generation rate in terms of the temperatures and pressures (with reference to Figure 1). The entropy generation rate for each component is added and is shown in block brackets.

$$\dot{W}_{net} = -T_0 \dot{S}_{gen} + \left(1 - \frac{T_0}{T*} \right) \dot{Q}* + \dot{m} c_{p0} (T_1 - T_{11}) - \dot{m} T_0 c_{p0} \ln (T_1 / T_{11}) \tag{20}$$

where

$$\begin{aligned}
\dot{S}_{gen} = & \left[-\dot{m} c_{p0} \ln (T_1 / T_2) + \dot{m} R \ln (P_1 / P_2) \right]_{compressor} \\
& + \left[\dot{Q}_0 / T_0 + \dot{m} c_{p0} \ln (T_3 / T_2) - \dot{m} R \ln (P_3 / P_2) \right]_{Duct\,23} \\
& + \left[\dot{m} c_{p0} \ln \left[\frac{T_{10} T_4}{T_9 T_3} \left(\frac{P_{10} P_4}{P_9 P_3} \right)^{(1-k)/k} \right] + \dot{Q}_0 / T_0 \right]_{recuperator} \\
& + \left[\dot{Q}_0 / T_0 + \dot{m} c_{p0} \ln (T_5 / T_4) - \dot{m} R \ln (P_5 / P_4) \right]_{Duct\,45} \\
& + \left[-\frac{\dot{Q}*}{T*} + \frac{\dot{Q}_{loss}}{T_0} + \dot{m} c_{p0} \ln (T_6 / T_5) - \dot{m} R \ln (P_6 / P_5) \right]_{receiver} \\
& + \left[\dot{Q}_0 / T_0 + \dot{m} c_{p0} \ln (T_7 / T_6) - \dot{m} R \ln (P_7 / P_6) \right]_{Duct\,67} \\
& + \left[-\dot{m} c_{p0} \ln (T_7 / T_8) + \dot{m} R \ln (P_7 / P_8) \right]_{turbine} \\
& + \left[\dot{Q}_0 / T_0 + \dot{m} c_{p0} \ln (T_9 / T_8) - \dot{m} R \ln (P_9 / P_8) \right]_{Duct\,89}
\end{aligned} \tag{21}$$

Note that $\dot{Q}^* - \dot{Q}_{loss} = \dot{Q}_{net}$.

2.6.3. Constraints

The concentration ratio between concentrator area and receiver aperture area, *CR* is constrained to CR_{min}.

$$D_{h,rec} L_{rec} / 8 - A_{s,conc} / CR_{\min} \leq 0 \quad (22)$$

Equation (23) prevents the receiver from losing its cavity shape, by only allowing a minimum of two diameters in the distance between the aperture edge and the edge of the receiver.

$$2D_{h,rec} - \left(\left(\sqrt{3}-1\right)/2\right)\sqrt{D_{h,rec} L_{rec} / 2\pi} \leq 0 \quad (23)$$

The cavity receiver tubes are constructed from copper. The maximum surface temperature of the receiver tubes should stay well below its melting temperature. A maximum receiver surface temperature of $T_{s,max}$ is identified for the analysis [27,29]. The surface area of a tube and the Dittus-Boelter equation [35] help to construct equation (24), which is the maximum surface temperature of the receiver.

$$T_{s,\max} = T_6 + \dot{Q}_{net} / \left(0.023 \pi L_{rec} k \, \mathrm{Pr}^{0.4} \left(4\dot{m} / \left(\mu \pi D_{h,rec}\right)\right)^{0.8}\right) \quad (24)$$

The longer the recuperator the more beneficial it is to the system. There needs to be a constraint on its length. To make sure the system stays compact, the recuperator's length should not exceed the length of the radius of the dish,

$$L_{reg} \leq D_{conc} / 2 \quad (25)$$

3. RESEARCH METHODOLOGY

There are five geometric variables to be optimised: The cavity receiver tube diameter, D_{rec}, the tube length of the cavity receiver, L_{rec}, the hydraulic diameter of the recuperator channels, $D_{h,reg}$, the length of the recuperator channels, L_{reg}, and aspect ratio of the recuperator channels, a/b_{reg}. The objective function (net power output of the system) in terms of the scaled geometry variables, parameters and constants is maximised using the dynamic trajectory optimisation method by Snyman [28] in MATLAB, with unit step size and convergence tolerance of 1×10^{-7}. The optimisation algorithm, LFOPC [28], requires the gradient of the objective function in each variable. The gradient of the objective function for each of the five variables in vector *X*, can be obtained with the derivative function where the step size, $h = 1 \times 10^{-8}$. Optimisation of the geometry variables was done for each combination of the following parameters: a range of parabolic dish diameters (D_{conc} = 6 – 18 m) and a range of micro-turbines from Garrett [29] (*MT* = 1 – 45) each having its own operating range (along the line of highest compressor efficiency on the compressor map of a specific micro-turbine).

A data point was created at each micro-turbine pressure ratio (in increments of 0.1) for each of the above combinations. Each data point represents an optimised system – a system with maximum net power output and optimised receiver and recuperator geometries. In Table 1 the default values are given, for which these results were generated. The effect on the optimum system, when each of these constants is changed individually, is also investigated for a system using *MT* = 32, and D_{conc} = 12 m. Note that when the receiver aperture lies in the horisontal plane, the receiver inclination is 90°.

Table 1 Values used for default analysis and for inspection.

Environmental condition or parameter	Symbol	Default	D_{conc} = 12 m, *MT* = 32
Surrounding temperature	T_0	300 K	288 K
Atmospheric pressure	P_1	80 kPa	100 kPa
Irradiance	I	1 000 W/m^2	800 W/m^2
Wind factor	w	1	10
Concentrator rim angle	φ_{rim}	45°	30°
Receiver inclination	β	90°	60°
Concentrator error	e_p	0.0067 rad	0.035 rad
Maximum receiver surface temperature	$T_{s,\max}$	1 200 K	1 100 K
Specular reflectivity	$refl$	0.93	0.8
Recuperator material conductivity	k	401 W/mK	237 W/mK
Recuperator height	H	1 m	2 m
Maximum recuperator length	$L_{reg,\max}$	D_{conc}/2	D_{conc}
Minimum concentration ratio	$CR_{\min}$	100	1 000

4. RESULTS

Figure 5 shows the maximum net power output, minimum internal and external irreversibility rates and maximum net absorbed heat rate for different operating conditions of micro-turbine 41 with a concentrator diameter of 16 m. Note that the default constants in Table 1 were used. The maximum net power output of the system at each operating condition (mass flow rate), was found by optimising the geometry variables to maximise the objective function. One can see that the highest (global) maximum net power output and the lowest minimum irreversibility or minimum entropy generation (global) rates are at the same operating point. This result is in agreement with the second law of thermodynamics. Note how the maximum net power output increases as the minimum irreversibility rates decrease as a function of mass flow rate. The highest maximum

net power output is at the point where the minimum irreversibility rate ($\dot{I}_{ext,\min} + \dot{I}_{\text{int},\min}$) is the lowest.

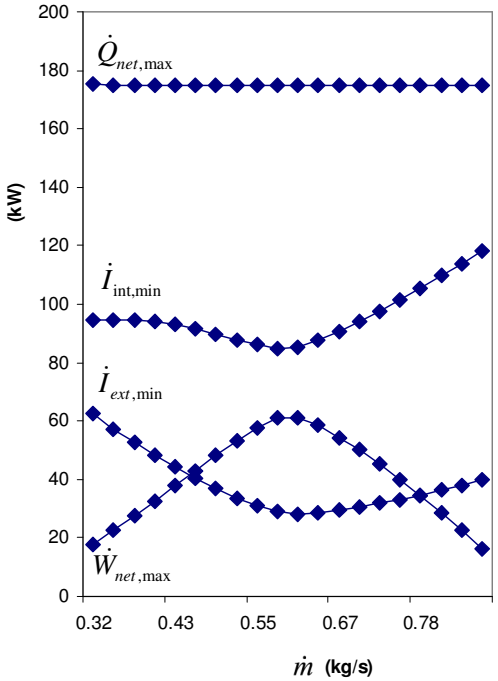

Figure 5 Maximum net power output and minimum irreversibility rates for D_{conc} = 16 m with MT = 41.

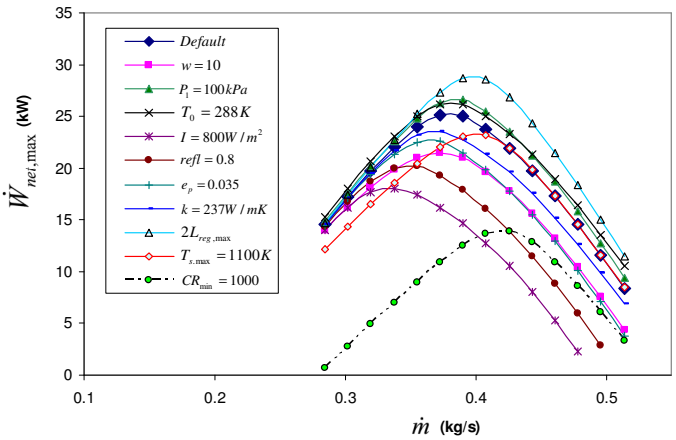

Figure 6 Change in maximum net power output for system using MT = 32 and D_{conc} = 12 m.

Each of the values in Table 1 is used to investigate its effect on the optimum geometry and operating conditions of the system. Figure 6 shows the maximum net power output for micro-turbine 32 with D_{conc} = 12 m, where the results using the default settings and changed constants are compared. It is concluded that a temperature decrease and pressure increase of the surroundings increase the maximum net power output. The decrease in maximum net power output due to wind, decreased specular reflectivity, concentrator error, recuperator material conductivity and increased concentration ratio minimum are shown. A higher concentration ratio decreases the maximum net power output because the size of the receiver decreases as the concentration ratio increases. The results shown in Figure 6 are expected to be similar for all the other configurations of concentrator diameter and micro-turbine.

A decrease in rim angle and receiver inclination makes no difference to the maximum net power output. It does, however, make a big change in the optimum receiver geometry variables. For a lower maximum allowable receiver temperature, the maximum net power output is lower. The increase of recuperator length and irradiance results in an increase in maximum net power output. The change in recuperator height makes no difference to the maximum net power output, but it changed the optimum dimensions of the recuperator.

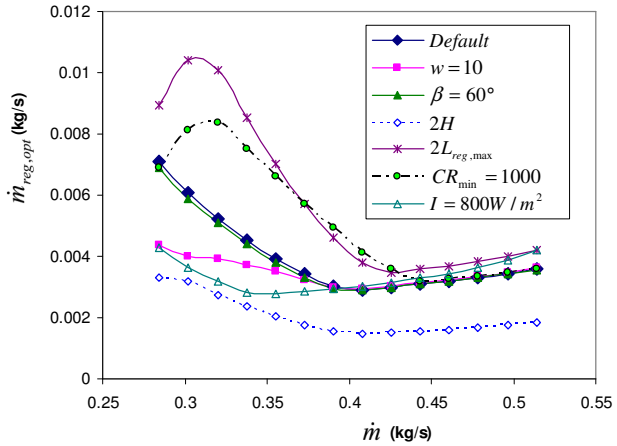

Figure 7 Optimum recuperator channel mass flow rate with changes in constants for D_{conc} = 12 m with MT = 32.

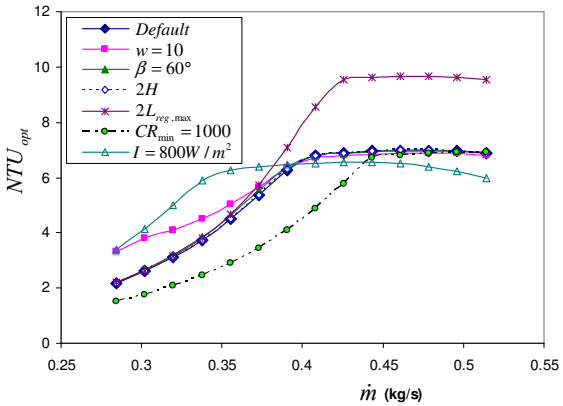

Figure 8 The optimum recuperator *NTU* with specific scenarios for D_{conc} = 12 m and MT = 32 for changed constants.

The effect of a few selected constants on the optimum mass flow rate of a recuperator channel is shown in Figure 7. A lowest optimum recuperator mass flow rate exists. Note how this minimum is shifted due to the constants.

In Figure 8 the optimum recuperator *NTU* is shown for D_{conc} = 12 m with micro-turbine 32. The extended recuperator length increases the maximum of the optimum *NTU*. The effect of the wind was to increase the optimum *NTU* slightly at lower system mass flow rates. The effect of higher minimum concentration ratio was to decrease the optimum *NTU* at smaller mass flow rates. The effect of irradiance at lower mass flow rates was to increase the optimum *NTU* as the irradiance

decreased. At higher mass flow rates, the effect was opposite. The other changes did not affect the optimum *NTU* much.

Note that the highest maximum net power output for the default settings in Figure 6 is at a mass flow rate of 0.375 kg/s. When looking at the optimum operating conditions of these mass flow rates, the net power output is not necessarily a maximum when the *NTU* is at its highest. This confirms that an optimum condition for an individual component in a system does not necessarily guarantee an optimum net power output, as was emphasised from the literature.

It is interesting to note that, in some cases, the system property curves do not differ from the default curves and in other cases they differ a lot. A 60° inclination (Figure 8) does not do much to the shape of the optimum *NTU* but it does, however, change the optimum geometry variables of the system. When considering Figure 6 again, the effect due to receiver inclination and recuperator height is not shown. Note that if the curve for a changed constant is not shown in a figure, it means that it was found to be the same as the default. The system geometry variables were altered (the irreversibilities were correctly spread) so that the system can still provide the same maximum net power output for the system with inclined receiver or altered recuperator height. The devastating effect of wind on the system, however, is shown in these figures. The system variables were not able to 'save' the maximum net power output.

Consider the default values given in Table 1. For all the optimised data points (all D_{conc}, and all operating points of all the micro-turbines), the optimum recuperator channel mass flow rate behaved in a specific way relative to the mass flow rate of the system. The behaviour of the optimum mass flow rate of the recuperator is shown in Figure 9 (showing only D_{conc} = 8, 12 and 16 m). Note the similarity between Figures 7 and 9. Take note that each data point in Figure 9 has an optimum geometry and gives maximum net power output at its specific mass flow rate. When inspecting Figure 10, (again, D_{conc} = 6, 10, 14 and 18 m are not shown, but behaved similarly), it can be concluded that, for all the data points, the optimum *NTU* increases as the system mass flow rate increases until it reaches its maximum. This means that it is most beneficial for a system with a small mass flow rate to have a small *NTU*. The following paragraph explains why. Also note the similarity between Figures 8 and 10.

The results of a system with *MT* = 41 is considered because the micro-turbine has a very large operating range in which the compressor efficiency is a maximum. Understanding the behaviour of this micro-turbine is very helpful in understanding Figures 9 and 10. The minimum internal and external irreversibility rates are shown for D_{conc} = 16 m with micro-turbine 41 in Figure 5. This distribution was found to be similar for all the combinations of concentrator diameters and micro-turbines optimised in this analysis.

Consider the point where the minimum external irreversibility rate, $\dot{I}_{ext,\min}$, is at its highest (Figure 5). $\dot{I}_{ext,\min}$ seems to be at a maximum when the mass flow rate is small.

$$\dot{I}_{ext} = \dot{m}c_{p0}(T_1 - T_{11}) - \dot{m}T_0 c_{p0} \ln(T_1/T_{11}) \qquad (26)$$

From equation (26) it follows that, for high external irreversibilities, T_{11} must be high, which means that the recuperator efficiency should be small. This is why the optimum *NTU* is small at small mass flow rates, as shown in Figure 10. The optimum *NTU* increases as the mass flow rate increases. The maximum recuperator length constraint is reached at around 0.25 kg/s for the D_{conc} = 12 m in Figure 9. After the length constraint is reached, the recuperator mass flow rate decreases as the mass flow rate increases to ensure an increase in *NTU* as the system mass flow rate increases.

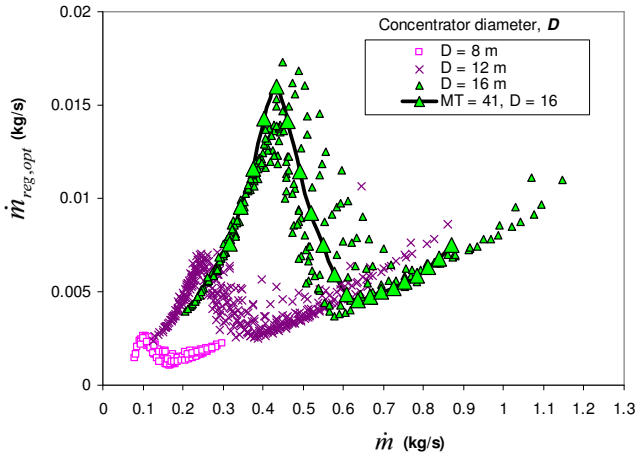

Figure 9 Optimum recuperator channel mass flow rate (D_{conc} = 8, 12 and 16 m).

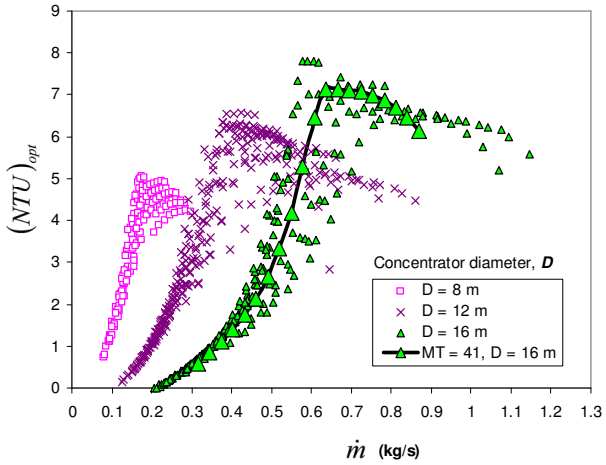

Figure 10 Optimum *NTU* for all data points (D_{conc} = 8, 12 and 16 m).

Consider the point where $\dot{I}_{ext,\min}$ is at a minimum (Figure 5). T_{11} will be at a minimum and the recuperator efficiency will be at a maximum. As $\dot{I}_{ext,\min}$ increases slightly with mass flow rate, the optimum *NTU* decreases slightly as shown in Figure 8. At the highest optimum *NTU* point, the recuperator channel mass flow rate is again utilised to be increased as the system mass flow rate increases in order to keep the optimum *NTU* at its maximum. In most of the cases (but not all cases), the highest maximum net power output in the operating range of

the micro-turbine was found at a mass flow rate close to the point of highest optimum *NTU* or at higher mass flow rates.

In Figure 11 it is shown that the maximum receiver surface temperature of the optimised data stays constant as a function of mass flow rate at small mass flow rates. This is due to the maximum surface temperature constraint of 1 200 K (for the default). At higher mass flow rates, the maximum surface temperature of the optimised data decreases as a function of mass flow rate. The larger the concentrator diameter, the larger the mass flow rate at which the maximum surface temperature would start decreasing.

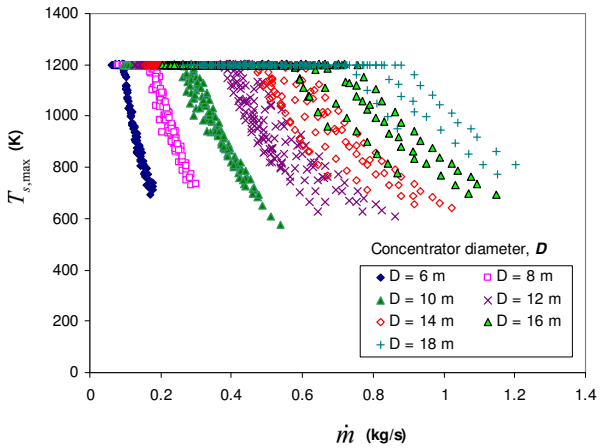

Figure 11 Maximum receiver surface temperature of all the optimised data points (all micro-turbines and each of its operating conditions).

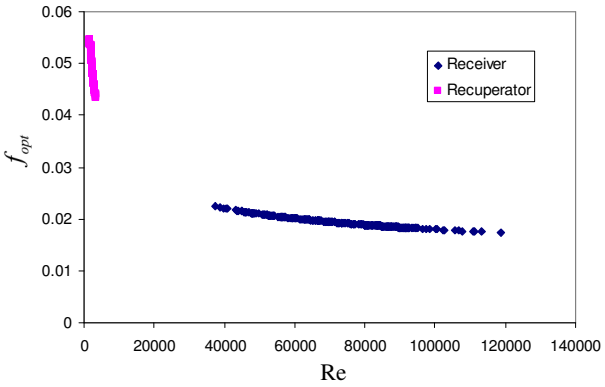

Figure 12 Optimum friction factor in receiver and recuperator for D_{conc} = 16 m.

The optimum friction factor of the receiver and recuperator channels, as a function of Reynolds number, is shown in Figure 12 for systems with different micro-turbines and operating mass flow rates with D_{conc} = 16 m. It is optimum for the recuperator to operate in the laminar flow regime while the receiver operates in the turbulent flow regime.

From the results (also shown in Figure 5) it follows that the largest maximum net power output for a system (or optimum operating point) is at a point where the internal irreversibility rate is approximately three times larger than the external irreversibility rate. This result can be approximated with equation (27) for all optimisation results in this analysis (with different concentrators and micro-turbines) where an optimum operating condition was found:

$$-T_0\left[\dot{S}_{gen}\right]_{\text{int,min}} \approx C_W\left[\dot{m}c_{p0}(T_1 - T_{11}) - \dot{m}T_0 c_{p0}\ln(T_1/T_{11})\right]_{ext,\text{min}} \qquad (27)$$

where $C_W = \dot{I}_{\text{int,min}} / \dot{I}_{ext,\text{min}} \approx 3$.

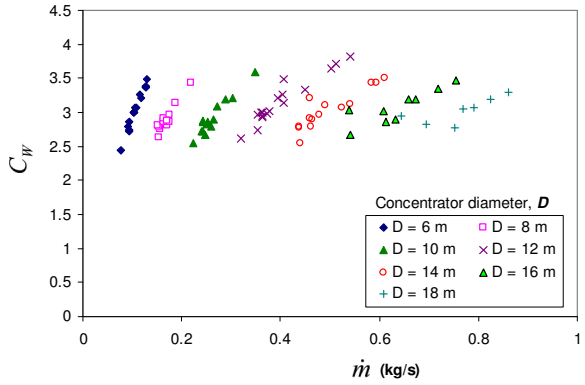

Figure 13 C_W as a function of the system mass flow rate.

Figure 13 shows that C_W mostly increases as the system mass flow rate increases. The rate of increase decreases as the concentrator diameter increases. Figure 13 shows that $2.4 \le C_W \le 4$, depending on the mass flow rate and concentrator diameter. Other data points which are not at an optimum operating point (or highest maximum net power output), or close to one, do not fall in this range. These results could be considered in the preliminary stages of the design of an open and direct solar thermal Brayton cycle.

5. CONCLUSION

The small-scale open and direct solar thermal Brayton cycle with recuperator has several advantages, but the main disadvantages of this cycle are the pressure losses in the recuperator and receiver, turbomachine efficiencies and recuperator effectiveness, which limit the net power output of such a system. In this work, a modified cavity receiver and a counterflow plate-type recuperator were optimally sized so that the solar thermal power system can have maximum net power output at a steady-state condition. A sizing algorithm was used to establish the net absorbed heat rate of the cavity receiver as a function of the receiver aperture diameter for a specific concentrator diameter with fixed focal length and rim angle. As a result, a specific geometry of the cavity receiver would fix the amount of power absorbed.

Off-the-shelf micro-turbines, operating in their range of maximum compressor efficiency, were considered in the analysis. The operating point in the range of maximum compressor efficiency, specific micro-turbine used and concentrator diameter were used as parameters in the analysis. For each set of parameters an objective function, the net power output, was maximised by optimising geometry variables of the modified cavity receiver and counterflow plate-type recuperator. This optimisation was done with limiting constraints. The dynamic trajectory optimisation method for

constrained optimisation was used. The net power output of the system was described in terms of the total entropy generation within the system.

Optimum system operating conditions were established in the analysis. The optimum recuperator channel mass flow rate and optimum *NTU* behaved very specifically with the system mass flow rate. The effects of various conditions such as wind, receiver inclination, concentrator rim angle and irradiance on the maximum net power output and optimum operating conditions of the system were investigated. Results showed that, for a specific environment and set of parameters, an optimum receiver and recuperator geometry exists so that the system can produce maximum net power output.

It was found that it is best for the receiver to operate in the turbulent flow regime, and for the recuperator channels to operate in the laminar flow regime. Results showed that at higher mass flow rates, the maximum receiver surface temperature decreased as a function of mass flow rate.

The irreversibilities were spread throughout the system in such a way that the minimum internal irreversibility rate was almost three times the minimum external irreversibility rate for all data points, which gave the highest maximum net power output of a micro-turbine. These results can be considered in the preliminary stages of design.

REFERENCES

[1] Chen L., Zhang, W. and Sun, F., Power, efficiency, entropy-generation rate and ecological optimization for a class of generalized irreversible universal heat-engine cycles, *Applied Energy*, Vol. 84, 2007, pp. 512-525.

[2] Mills, D., Advances in solar thermal electricity technology, *Solar Energy*, Vol. 76, 2004, pp. 19-31.

[3] Stine, B.S. and Harrigan, R.W., *Solar Energy Fundamentals and Design*, John Wiley & Sons, Inc., New York, 1985.

[4] Bejan, A., *Entropy Generation through Heat and Fluid Flow*, John Wiley & Sons, Inc., Colorado, 1982.

[5] Bejan, A., Method of entropy generation minimization, or modeling and optimization based on combined heat transfer and thermodynamics, *Rev Gén Therm*, Vol. 35, 1996, pp. 637-646.

[6] Bejan, A., *Advanced Engineering Thermodynamics, 2nd ed*, John Wiley & Sons, Inc., Durham, 1997.

[7] Bejan, A., Tsatsaronis, G. and Moran, M., *Thermal design and optimization*, John Wiley & Sons, Inc., New York, 1996.

[8] Ordóñez, J. C. and Bejan, A., Entropy generation minimization in parallel-plates counterflow heat exchangers, *International Journal of Energy Research*, Vol. 24**,** 2000, pp. 843-864.

[9] Shiba, T. and Bejan, A., Thermodynamic optimization of geometric structure in the counterflow heat exchanger for an environmental control system, *Energy*, Vol. 26, 2001, pp. 493-511.

[10] Zimparov, V. D., Da Silva, A.K. and Bejan, A., Thermodynamic optimization of tree-shaped flow geometries with constant channel wall temperature, *International Journal of Heat and Mass Transfer*, Vol. 49, 2006, pp. 4839-4849.

[11] Zimparov, V. D., Da Silva, A.K. and Bejan, A., Thermodynamic optimization of tree-shaped flow geometries, *International Journal of Heat and Mass Transfer*, Vol. 49**,** 2006, pp. 1619-1630.

[12] Petela, R., *Engineering Thermodynamics of Thermal Radiation*, McGraw-Hill, New York, 2010.

[13] Joshi, A. S., Dincer, I. and Reddy, B.V., Development of new solar exergy maps, *International Journal of Energy Research*, Vol. 33, 2009, pp. 709-718.

[14] Ratts, B. E. and Raut, A.G., Entropy generation minimization of fully developed internal flow with constant heat flux, *Journal of Heat Transfer*, Vol. 126(4), 2004, pp. 656-659.

[15] Sarangi, S. and Chowdhury, K., On the generation of entropy in a counterflow heat exchanger, *Cryogenics*, Vol. 22(2), 1982, pp. 63-65.

[16] Cornelissen, R. L. and Hirs, G.G., Exergetic optimization of a heat exchanger, *Energy Conversion and Management*, Vol. 1(15-17), 1997, pp. 1567-1576.

[17] Zimparov, V., Extended performance evaluation criteria for enhanced heat transfer surfaces: heat transfer through ducts with constant heat flux, *International Journal of Heat and Mass Transfer*, Vol. 44(1), 2001, pp. 169-180.

[18] Hesselgreaves, J. E., Rationalisation of second law analysis of heat exchangers, *International Journal of Heat and Mass Transfer*, Vol. 43(22), 2000, pp. 4189-4204.

[19] Oğulata, R. T., Doba, F. and Yilmaz, T., Irreversibility analysis of cross flow heat exchangers, *Energy Conversion & Management*, Vol. 41(15), 2000, pp. 1585-1599.

[20] Shuai, Y., Xia, X. and Tan. H., Radiation performance of dish solar concentrator/cavity receiver systems, *Solar Energy*, Vol. 82, 2008, pp. 13-21.

[21] Prakash, M., Kedare, S. B. and Nayak, J. K., Investigations on heat losses from a solar cavity receiver, *Solar Energy*, Vol. 83, 2009, pp. 157-170.

[22] Sendhil Kumar, N. and Reddy, K. S., Comparison of receivers for solar dish collector system, *Energy Conversion and Management*, Vol. 49, 2008, pp. 812-819.

[23] Sendhil Kumar, N. and Reddy, K. S., Numerical investigation of natural convection heat loss in modified cavity receiver for fuzzy focal solar dish concentrator, *Solar Energy*, Vol. 81, 2007, pp. 846–855.

[24] Reddy, K. S. and Sendhil Kumar, N., Combined laminar natural convection and surface radiation heat transfer in a modified cavity receiver of solar parabolic dish, *International Journal of Thermal Sciences*, Vol. 47, 2008, pp. 647–1657.

[25] Reddy, K. S. and Sendhil Kumar, N., An improved model for natural convection heat loss from modified cavity receiver of solar dish concentrator, *Solar Energy*, Vol. 83, 2009, pp. 1884–1892.

[26] Jubeh, N. M., Exergy analysis and second law efficiency of a regenerative brayton cycle with isothermal heat addition, *Entropy*, Vol. 7(3), 2005, pp. 172-187.

[27] Shah, R. K., Micro Gas Turbines, 2, *Compact Heat Exchangers for Microturbines,* Neuilly-sur-Seine, France: RTO, 2005, pp. 2-1 – 2-18. Available from: http://www.rto.nato.int/abstracts.asp.

[28] Snyman, J.A., The LFOPC leap-frog algorithm for constrained optimization, *Computers and Mathematics with Applications*, Vol. 40, 2000, pp. 1085-1096.

[29] Garrett, Garrett by Honeywell: turbochargers, intercoolers, upgrades, wastegates, blow-off valves, turbo-tutorials, 2009, Available at: http://www.TurboByGarrett.com [Accessed 26 April 2010].

[30] Burden, R. L. and Faires, J. D., *Numerical Analysis, 8th ed*, Thomson Brooks/Cole, Youngston State University, 2005.

[31] Gnielinski, V., New equations for heat and mass transfer in turbulent pipe and channel flow, *International Chemical Engineering*, Vol. 16, 1976, pp. 359-368.

[32] Petukhov, B. S., Heat transfer and friction in turbulent pipe flow with variable physical properties, *Advances in Heat Transfer*, Vol. 6, 1970.

[33] Çengel, Y. A., *Heat and Mass Transfer, 3rd ed*, McGraw-Hill, Nevada, Reno, 2006.

[34] Snyman, J. A., *Practical Mathematical Optimization*, University of Pretoria, Pretoria, 2009.

[35] Dittus, F. W. and Boelter, L. M. K., University of California publications on engineering, Vol.2, 1930, pp. 433.